Nanoscale Advances

ROYAL SOCIETY OF CHEMISTRY

PAPER

View Article Online
View Journal | View Issue

Cite this: *Nanoscale Adv.*, 2025, **7**, 621

Electrostatic adsorptive loading of ciprofloxacin and metronidazole on chitosan nanoparticles to prolong the drug delivery process with preserved antibacterial activities: formulation and characterization

Fatema Tuj Jahura,[ab] Farhana Khanam Ferdousi,[b] Abu Hena Mostofa Kamal,[c] Anwar Ul-Hamid,[d] Md. Qamrul Ehsan[b] and Mohammad Abul Hossain *[b]

This study presents the formulation and evaluation of chitosan-based homogeneous nanoparticles of ciprofloxacin (CP) and metronidazole (MTZ) with improved loading efficiency to enhance the controlled release of drug within the human body as well as for the enhancement of the antibacterial activity. The drug-loaded chitosan nanoparticles (CSNPs) were prepared using deacetylated chitosan extracted from shrimp shells. The characterization of the drug-loaded CSNPs were performed by FTIR, XRD, SEM and TEM analyses. The association efficiencies of the drug-loaded CSNPs were found to be 93% ± 3% and 89% ± 3% for ciprofloxacin and metronidazole, respectively. TEM analysis confirmed the formation of homogeneous nano-sized particles of 0.1–1.0, 0.3–1.3, and 0.4–1.5 nm for CSNPs, CP-CSNPs and MTZ-CSNPs, respectively, which elucidated the adsorptive loading of the drug molecules on the surface of the chitosan nanoparticles. A comparison of the surface charges of the above nanoparticles suggested that the electrostatic adsorption dominated the drug loading process. Both of the drug-loaded CSNPs showed sustained release of drugs after an initial rapid release in the *in vitro* release kinetic studies. Thus, the adsorption of drugs on the surface of CSNPs resulted in the sustained release of the drugs from CSNPs without encapsulation. Positive results of the antibacterial activities of the CP-loaded CSNPs (CP-CSNPs) against both Gram-positive and Gram-negative bacteria were observed.

Received 4th July 2024
Accepted 11th November 2024

DOI: 10.1039/d4na00548a

rsc.li/nanoscale-advances

1. Introduction

The effectiveness of a large number of medicines is frequently limited by their ability to get to the target site for therapeutic intervention.[1] In the case of a normal dosage volume, only a very small amount of the administered dose reaches the target site, while the maximum portion of the dose is dispersed in every part of the rest of the body according to its biochemical and physicochemical properties. Therefore, it is necessary to develop a drug administration system that optimizes the pharmaceutical performance of a drug, thereby reducing its toxic side effects.

Controlled drug delivery increases the availability of the administered doses of drugs within the therapeutic window or at the target site for a sustained period of time. Nevertheless, this is difficult to achieve in the case of traditional drug delivery systems. In a controlled drug delivery system, drugs can be protected from degradation *in vivo*, which improves their half-life and also their therapeutic effects. To establish a controlled drug delivery system, the drug is incorporated into the carrier first. Then, after administration, the carrier system can release the drug over a sustained period of time, ranging from days to months.[2]

In the case of drug administration systems, nanoparticles have attracted much attention from pharmaceutical scientists since 1990 due to their various advantages, like controlled drug release, lesser frequency of dose administration and protection from *in vivo* chemical degradation of drugs.[3,4] As a consequence, breathtaking improvements have been observed in patient compliance. Polymeric materials like chitosan have a long history of use in synthesizing biodegradable nanoparticles (CSNPs) for diverse applications (like biocatalyst encapsulation, wastewater treatment, food preservative and metal nanocomposites) due to their small size,[5] high surface area,[6] high stability and quantum size effect.[7] In addition, the non-toxicity, non-antigenicity and good biocompatibility of chitosan

[a]*Institute of Nuclear Science and Technology, Atomic Energy Research Establishment, Bangladesh Atomic Energy Commission, Dhaka-1349, Bangladesh*
[b]*Department of Chemistry, Faculty of Science, University of Dhaka, Dhaka-1000, Bangladesh. E-mail: hossainabul@yahoo.com; hossainabul@du.ac.bd*
[c]*Institute of Food and Radiation Biology, Atomic Energy Research Establishment, Bangladesh Atomic Energy Commission, Dhaka-1349, Bangladesh*
[d]*Core Research Facilities, King Fahd University of Petroleum & Minerals, Dhahran 31261, Saudi Arabia*

nanoparticles (CSNPs) make them an ideal component for different biomedical and pharmaceutical applications, like molecular imprinting, pharmaceutical formulations and so on.[8–13] In recent years, CSNPs have attracted particular attention for drug transportation because of their exotic ability to target specific tissues and enable controlled drug release. Many chitosan-controlled drug distribution systems have been developed in recent times through the chemical modification of functional groups in chitosan (chitosan derivatives), which ultimately upgrades the bioactivity and aqueous solubility of chitosan. However, such chemical modification does not affect the inherent properties of chitosan, but rather magnifies its scope of applications for a wide range of chemicals in multiple environments (acidic, alkaline, or neutral conditions). The administration system of many antibiotics (like ampicillin, doxycycline, and ceftriaxone) and anti-cancer drugs (such as 5-fluorouracil, paclitaxel, doxorubicin, letrozole, and saponin) have been extensively studied using CSNPs as a potential drug transporter. This research project was also focused on this field, with detailed investigations of the prolonged drug delivery process of two leading antibiotics, ciprofloxacin and metronidazole, loaded with chitosan nanoparticles. In a nutshell, the paper aimed to address the gap in the existing research on these two antibiotics.

Ciprofloxacin is a commonly used oral antimicrobial drug whose broad spectrum of activity means it has the potential to treat serious infections caused by Gram-negative and Gram-positive bacteria. However, it is a poorly cell-penetrating antibiotic since it is almost insoluble in aqueous medium and only slightly soluble in organic solvents, such as ethanol and methylene chloride.[14] The problem of its lower drug solubility can be avoided and its bioavailability improved by formulating the drug in systems containing colloidal drug transporters, such as biodegradable polymeric nanoparticles. So far, various research groups have already reported ciprofloxacin-loaded different synthetic biodegradable polymeric nanoparticles for the sustained release of this antibiotic.[15–17] Nevertheless, some of these biodegradable polymeric nanoparticles have concerns regarding toxicity.[18] On the other hand, Jain and Banerjee[19] showed that non-toxic natural polymer chitosan NPs can act as promising carriers for constant ciprofloxacin release in infective conditions in a controlled way. They prepared ciprofloxacin hydrochloride-loaded CNPs by the conventional ionotropic gelation method with tripolyphosphate anions to develop single-dose-delivery systems for the extended antibiotic release of this drug. Nevertheless, the major drawbacks of their study was the poor drug encapsulation of ciprofloxacin with CNPs (only 35.01% $\pm$ 2.66%; drug-to-carrier ratio of 0.5 : 1; and average particle sizes of 247 $\pm$ 48 to 322 $\pm$ 52 nm for CSNPs). Later on, Ibrahim *et al.* (2015)[20] further examined the ionic gelation of chitosan with tripolyphosphate (TPP) anions to optimize the particle size of CSNPs by varying the concentrations of chitosan and sodium (TPP) keeping the pH of the solution and ultrasonication time constant (at pH 5.5 and 45 min) for the intracellular delivery of ciprofloxacin. The results showed that the antibacterial activity of ciprofloxacin loaded with CSNPs increased with the increase in antibiotic concentration. However, the particle sizes were more favorable at the chitosan concentration of 0.2 g mL^{-1} (2–8 nm) at a constant concentration of TPP, while the size increased with the increase in TPP. However, the research lacked information regarding the encapsulation efficiency. Therefore, these gaps should be clarified and further detailed investigations in this area are desirable.

On the other hand, metronidazole is an amoebicide, antiprotozoan and antibiotic that is effective against anaerobic bowel amoebiasis, giardiasis, trichomoniasis, bacterial vaginosis, and surgical infections.[21] The development of colon-targeted metronidazole-loaded nanoparticles has attracted attention in recent years. The prime goal of using this drug transporter is to deliver the medication exactly to the colon for achieving an efficient effect against *E. histolytica*. However, the administration of this drug as a classic tablet provides a minimum amount of metronidazole for local action in the colon.[21,22] In fact, due to the presence of insoluble mucus hydrogel in our gastrointestinal tract, which is mainly glycoproteins made of ester sulfate and sialic acid groups, an overall strong net negative charge exists all over the gastrointestinal tract.[23] Therefore, a mucoadhesive-featured chitosan may be a potential drug transporter to deliver any drug to mucosal tissues in the gastrointestinal tract. This adhesion mechanism involves hydration, hydrogen bonding, or ionic interactions.[24–27] Elzatahry and Mohy Eldin (2008)[28] formulated a mucoadhesive chitosan containing metronidazole (MTZ) for colon-specific delivery using the ionic gelation method and succeeded in controlling the release of MTZ over a 12 h period (CSNPs size: 280–300 nm; chitosan/TPP = 4 : 1, drug-loaded nanoparticles sizes <300 nm). Nevertheless, a prominent linear relationship was observed between the chitosan/TPP weight ratio and the particle size, whereas, the mucoadhesive properties of chitosan were reduced with the increase in the concentration of antibiotic as well as the possible particle size. Therefore, further reduction of the size of the CSNPs through a modified process could be a new focus of much attention for scientists.

In the present work, chitosan nanoparticles containing ciprofloxacin and metronidazole were prepared separately, using a modified ionic gelation method to reduce the homogeneous size of the CSNPs and chitosan-loaded drugs, which should ultimately enhance the efficacy of these two drugs. This new perspective enabled a more sustained release of these two antibiotics. The mechanisms of drug loading and release were established from TEM study and surface charge measurements. Accordingly, the antibacterial activity of the antibiotic drug-loaded chitosan nanoparticles were evaluated against Gram-positive and Gram-negative bacterial strains.

2. Experimental

2.1. Materials

Chitosan was extracted from waste shrimp shell using a traditional method described elsewhere in the literature.[29] The physical characteristics of the obtained chitosan are summarized in Table 1. Sodium tripolyphosphate ($Na_5P_3O_{10}$) (Na-TPP), dimethyl sulfoxide [$(CH_3)_2SO$], and di-sodium hydrogen phosphate, (Na_2HPO_4) were obtained from Merck Germany. Glacial acetic acid (CH_3COOH) was purchased from Daejung Chemicals &

Table 1 Characteristics of the extracted chitosan[29]

Molecular formula	$(C_{18}H_{35}N_3O_{13})_n$
Molecular weight (g mol^{-1})	2.3×10^5
Solubility (%)	82.85 (soluble in pH 3–4)
Degree of deacetylation (%)	70

Metals Co. Ltd, Korea. In order to load drugs within the chitosan nanoparticles, ciprofloxacin was obtained from Reneta Pharmaceuticals Ltd, Bangladesh. Metronidazole was provided by ACI Pharmaceuticals Ltd Bangladesh, with a potency of 99%. The bacterial strains for the antimicrobial study were collected from the Veterinary Drug Residue Analysis Division and Institute of Food and Radiation Biology, IFRB, AERE, Savar, Dhaka, Bangladesh.

2.2. Preparation of the chitosan and drug-loaded chitosan nanoparticles

Chitosan nanoparticles (CSNPs) were prepared from extracted chitosan[29] with minor modifications of the ionic gelation method.[30] The characteristic features of the extracted chitosan are shown in Table 1. The parameters for the CSNPs preparation were optimized as described in a previous report.[29] In brief, the ionic crosslinking of 2% chitosan (in 1% acetic acid) with 1% aqueous sodium tripolyphosphate (Na-TPP) was performed under constant magnetic stirring for 30 min at room temperature. According to TEM analysis,[29] the prepared CSNPs with the smallest particle size (0.1–1.0 nm) were considered as the optimized formulation of CSNPs for the antibiotic drug loading.[29]

For assessing the association of each drug with CSNPs in the optimized formulation, it was added to the chitosan solution (2%) before adding the TPP solution in it. Then, 1% Na-TPP solution was added to the mixture in a chitosan to TPP weight ratio of 5 : 1 under continuous magnetic stirring. The reaction was kept for 30 min at room temperature to form a suspension of the drug-loaded CSNPs. In this case, the effect of the concentration of ciprofloxacin in the chitosan solution on the ciprofloxacin-loaded chitosan nanoparticles (CP-CSNPs) preparation in terms of the loading or association efficiency was investigated by changing the ratio of ciprofloxacin to chitosan as 0.5 : 1.0, 0.65 : 1.0, 0.8 : 1, and 1.0 : 1.0. In the case of MTZ loading, MTZ was added to chitosan solution in a MTZ to chitosan ratio of 0.5 : 1.0 before adding Na-TPP. Higher ratios of MTZ : chitosan were not chosen because of the low solubility of MTZ in chitosan solution at higher concentration. Then the antibiotics-loaded CSNPs were separated from the suspension by centrifugation and were then freeze-dried at −50 °C using a freeze drier (LABCONCO, USA).

2.3. Measurement of the drug loading efficiency

The association efficiency (AE) or drug loading efficiency (LE) indicates the efficiency of the preparation method as it expresses the total amount of drug within the nanoparticles. After separating the antibiotic drug-loaded CSNPs from the suspension, the amount of free drug in the supernatant was measured using a UV-spectrophotometer (UV-1800 Spectrophotometer, Shimadzu, Japan) at the appropriate wavelength for the respective drugs. The amounts of drugs loaded or associated were evaluated from the difference between the total quantity of drug added to the loading solution and the quantity of non-entrapped drug remaining in the supernatant. Finally, the association efficiencies (AE) of the nanoparticles were calculated using eqn (1).

$$\mathrm{AE}(\%) = \frac{T_{\mathrm{Ad}} - T_{\mathrm{f}}}{T_{\mathrm{Ad}}} \times 100 \quad (1)$$

where T_{Ad} is the total antibiotic drug used to prepare the nanoparticles and T_{f} is the free drug in the supernatant.

2.4. Characterization of the nanoparticles

Morphological characterization, and qualitative and quantitative elemental analyses of the nanoparticles were done using a field emission scanning electron microscopy system (FESEM) (JEOL JSM-7600F), equipped with an energy dispersive X-ray (EDX) unit. The samples for FESEM analysis were prepared by completely drying the sample and then coating with platinum in vacuum. Then the micrographs of the particles were captured by FESEM. The morphology and size characteristics of the unmodified CSNPs loaded with different drugs were also observed by transmission electron microscopy (TEM) (JEOL, JEM 21000F). The TEM samples were obtained using a pastor pipette to place a drop of the chitosan nanoparticle suspension onto carbon-coated copper grids. The samples were dried at room temperature and then examined without any further modification or negative staining. Fourier transform infrared (FTIR) spectra of the materials were recorded in the range of 400–4000 cm^{-1} on an IR Prestige-21 system (Shimadzu, Japan) with 4 cm^{-1} resolution using the potassium bromide (KBr) disk method. The crystalline phase of the nanoparticles was analyzed by powder X-ray diffraction (XRD) patterns using an XRD 7000 diffractometer (Shimadzu, Japan) equipped with Ni-filtered Cu-K$_\alpha$ radiation (λ = 1.5406 Å) operated at 40 kV and 40 mA. Diffraction patterns were recorded within the 2θ range of 5°–70° in the continuous mode. The surface charge or zeta potential of the prepared chitosan nanoparticles, ciprofloxacin-loaded chitosan, and metronidazole-loaded chitosan nanoparticles were measured as a function of pH by the acid–base titration method proposed by Parks *et al.*[31] and Hossain.[32]

2.5. Biomedical application of drug-loaded chitosan nanoparticles

2.5.1. *In vitro* release of drugs from the chitosan nanoparticles. The *in vitro* drug release profiles of CSNPs loaded with ciprofloxacin and metronidazole over time were investigated in phosphate-buffered saline (PBS) at pH 7.0 as blood serum. The CSNPs loaded with different antibiotics were suspended in 50 mL of PBS and then put in to a water bath shaker under the condition of 37 °C and 150 rpm. To determine the amount of free antibiotic in the release media at a certain time, 5 mL of the sample was withdrawn at that specific time and was transferred to another test tube. The volume of the main nanoparticles

suspension was kept constant by adding another 5 mL of fresh dissolution media to avoid saturation of the media. The process was repeated after each scheduled time interval. The antibiotic samples that were withdrawn at different time intervals were analyzed by UV spectrophotometry. The quantity of released drugs in the dissolution media at each scheduled time point was assessed by comparing the UV absorbance of the sample withdrawn at that time with a standard curve of absorbance *vs.* concentration of the series of diluted drug solutions in PBS.

2.5.2. Antibacterial activity analysis. The antibacterial activity of the ciprofloxacin-loaded chitosan nanoparticles (CP-CSNPs) was investigated against both Gram-positive and Gram-negative bacteria. The activities were analyzed using a disk diffusion assay. The minimum inhibitory concentration (MIC) and minimum bactericidal concentration (MBC) were also determined. In the disc diffusion assay, the test samples with specific concentrations were applied on sterile filter paper disks and the solvents from the disks were evaporated by keeping the disks in the oven at 40 °C for 1 h. Then the disks were placed gently on Muller Hinton agar (MHA) plates seeded with fresh bacterial culture and kept in a refrigerator at 4 °C for 2 h to diffuse the test samples from the disks to a considerable portion of the agar media. After that, the plates were incubated at 37 °C for 16 h, and the diameter of the zone of inhibition produced by each test sample was measured in mm.

2.5.3. Determination of MIC and MBC by the broth macrodilution method. MIC was determined by the macrodilution method described by Wiegand.[33] In brief, various dilutions of the test antibiotic drugs and drug-loaded chitosan nanoparticles samples were prepared in sterile Muller Hinton Broth (MHB) in the concentration range of 0.06–128 mg L^{-1}. Then 1.0 mL of each dilution was added to different test tubes for testing the bacterial isolates. For growth control and sterility control, the test tubes were filled with 1.0 mL of sterile MHB each without an antimicrobial agent and appropriately labeled. Then each of the test tube containing the sample solution and the growth control test tubes were inoculated with 1.0 mL of the bacterial suspensions and incubated at 37 °C, with shaking at

Table 2 Loading efficiency of CP and MTZ in different experimental formulations

No.	Drug : chitosan	AE of CP-CSNPs (%)	AE of MTZ-CSNPs (%)
1	0.5 : 1.0	83 ± 3	89 ± 3
2	0.65 : 1.0	90 ± 3	—
3	0.8 : 1.0	92 ± 3	—
4	1.0 : 1.0	93 ± 3	—

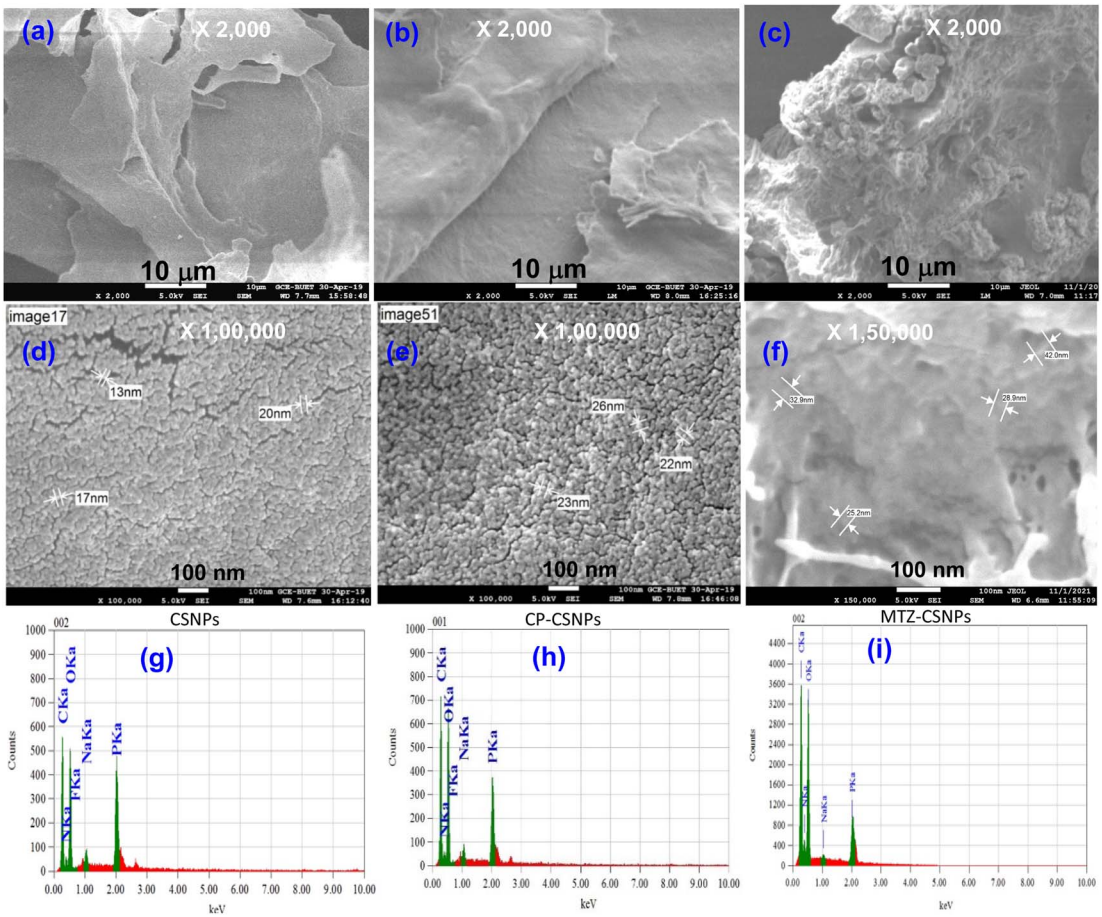

Fig. 1 SEM images of (a and d) CSNPs, (b and e) CP-loaded CSNPs, (c and f) MTZ-loaded CSNPs and EDX spectra of (g) CSNPs, (h) CP-loaded CSNPs (CP-CSNPs), and (i) MTZ-loaded CSNPs (MTZ-CSNPs).

225 rpm for 16 h. The tubes were then studied for visible signs of growth or turbidity. The lowest concentration of chitosan and nanoparticles that inhibited the growth of bacteria was considered as the minimum inhibitory concentration (MIC). The minimum bactericidal concentration (MBC) was determined by sub-culturing the organisms from the tubes used for the MIC test into fresh media and the lowest concentration at which no growth was observed was the MBC.

3. Results and discussion

3.1. Drug association efficiency

The association efficiencies (AEs) of CSNPs for CP and MTZ were determined using eqn (1). The average percentage association efficiencies of these formulations are shown in Table 2. From Table 2, it is seen that the loading process of ciprofloxacin was amount dependent, although the dependency was not very significant. An increase in ciprofloxacin concentration led to a slight increase in association efficiency. However, the ratios of 1.0 : 0.8 and 1 : 1 for chitosan : CP in the loading procedure resulted in almost no change in the association efficiency of ciprofloxacin (varying from 83 ± 3% to 93 ± 3%). Finally, the association efficiency of the CS4 formulation containing the CS : CP ratio of 1 : 1 was almost 93 ± 3%, which was the highest association efficiency and was due to electrostatic interaction between CS and CP, and thus, this formulation of CS4 was selected for further analysis.

In the case of MTZ, the metronidazole : chitosan ratio of 0.5 : 1.0 was selected for loading metronidazole within the chitosan nanoparticles because of the low solubility of metronidazole in chitosan solution at a higher concentration level. In addition, it was evident from the results of previous reports[34] that increasing the metronidazole concentration leads to a decrease in metronidazole loading on CSNPs. Finally, the percentage of AE was found to be 89%, which is satisfactory and higher than that of previous studies.[34]

3.2. Characterization of the nanoparticles

3.2.1. SEM analysis of the surface morphology. The SEM images of CSNPs without and with drugs are presented in Fig. 1(a–f) at different magnifications. The images displayed the uniform spherical shapes and aggregation of the particles with diameters of 13–20 nm (Fig. 1d). In Fig. 1e, the SEM image of the CP-CSNPs showed a spherical morphology with physical aggregation of nanoparticles 20–30 nm in size. It could also be seen in the SEM images of the MTZ-CSNPs that there was cluster of particles with diameters ranging from 25–45 nm and the particles were in the agglomerated state (Fig. 1f). Thus, the sizes of the CP-CSNPs and MTZ-CSNPs (Fig. 1d and f) in comparison to the blank one (Fig. 1d) were found to be increased, which indicated the possible adsorption of drugs on the surface of the CSNPs.

3.2.2. EDX analysis. The elemental composition of the drug-loaded CSNPs was investigated by EDX analysis, as shown in Fig. 1(g–i). The EDX spectrum (Fig. 1h) of the chitosan

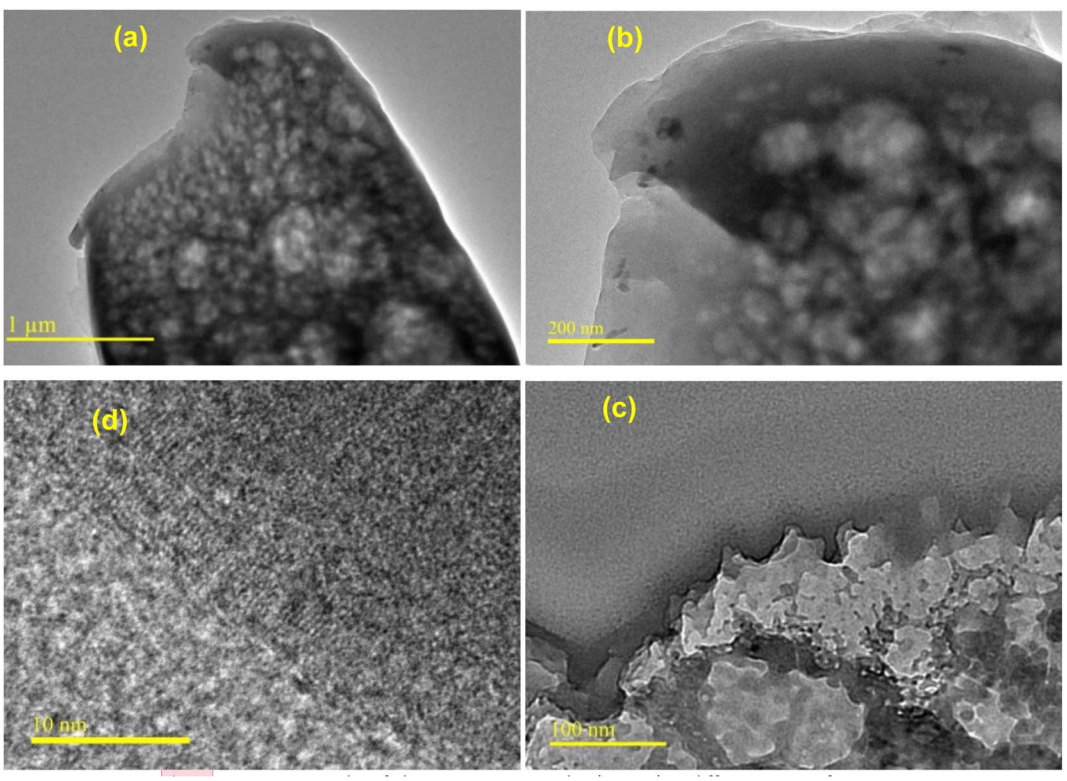

Fig. 2 TEM micrographs of chitosan nanoparticles (CSNPs) at different magnifications: (a) ×2000, (b) ×50 000, (c) ×100 000 and (d) ×300 000.

nanoparticles after ciprofloxacin loading presented a new peak corresponding to fluorine. The EDX analysis confirmed the presence of sodium and phosphorus with atomic weights of 0.65% Na and 3.24% phosphorus in the CP-CSNPs and 0.91% and 9.20% in the MTZ-CSNPs, suggesting the presence of TPP in the nanoparticles (Fig. 1h and i). Besides, the EDX spectrum showed signals for F, indicating the incorporation of ciprofloxacin into the chitosan nanoparticles (Fig. 1h). Comparing the EDX result of MTZ-CSNPs with the blank one, as presented in Fig. 1g, it could be seen that there is was a significant change in the atomic % of C, N, and O, which proved metronidazole was loaded into the chitosan nanoparticles. The EDX qualitative analysis also showed that there is no impurity element present in the nanoparticles.

3.2.3. TEM analysis. A more precise visualization of the size and morphology of CSNPs without and with drugs loaded was performed in a dried state by TEM, as shown in Fig. 2(a–d), 3(a–e) and 4(a–f) at different magnifications. Fig. 3(a1) shows the mixture of ciprofloxacin (CP) and chitosan nanoparticles (CSNPs), while Fig. 3(a2) shows ciprofloxacin individually, and Fig. 3(b–d) show the CP-loaded CSNPs at different magnifications, like as an adsorption of CP on the CSNPs surface. As shown in Fig. 3d, the CP-CSNPs possessed a regularly spherical shape and the particles were sized approximately 0.3–1.3 nm. From Fig. 2d, it could be seen that the size of the blank chitosan nanoparticles was 0.1–1.0 nm. This increase in size in the case of CP-CSNPs indicated that the CP drug was successfully associated with CSNPs by adsorption onto the surface of the nanoparticles. Fig. 3e shows the non-crystalline nature of the CP-CSNPs. Again, the TEM micrographs of the metronidazole-loaded chitosan nanoparticles (MTZ-CSNPs) at different magnifications are presented in Fig. 4(a–e), while Fig. 4(f) shows the non-crystalline nature of the MTZ-CSNPs. Fig. 4e shows the individual particle sizes of the MTZ-CSNPs was around 0.4–1.5 nm, which was also larger than that of the blank chitosan nanoparticles (0.1–1.0 nm) shown in Fig. 2d. A comparison of the particle size of the blank chitosan nanoparticles (CSNPs) with that of the individual CP and MTZ-loaded CSNPs is

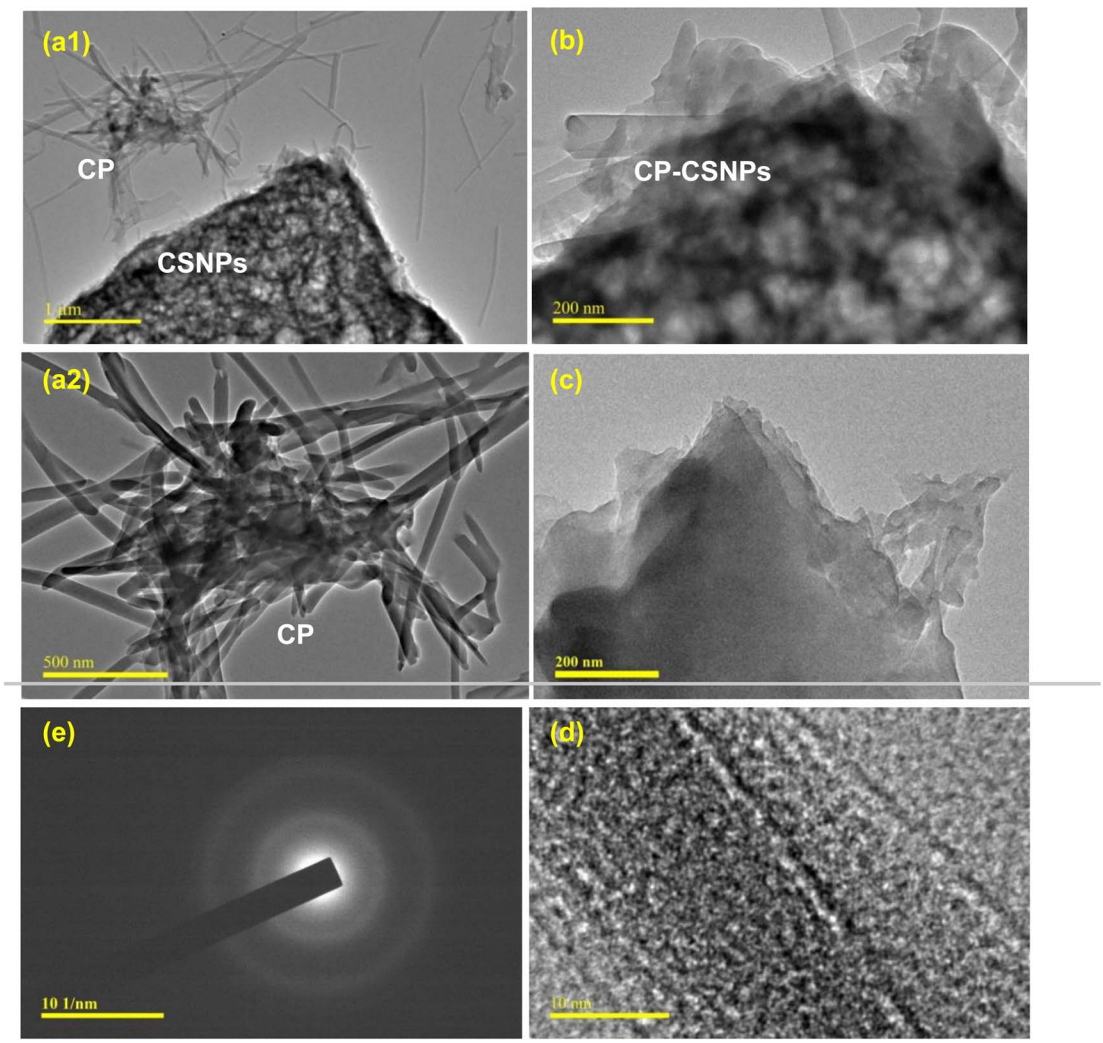

Fig. 3 TEM micrographs of ciprofloxacin (CP)-loaded chitosan nanoparticles (CP-CSNPs): (a1) mixture of CP and CSNPs, (a2) individual ciprofloxacin, (b–d) CP-loaded CSNPs at different magnifications, and (e) image showing the non-crystalline nature of the CP-CSNPs.

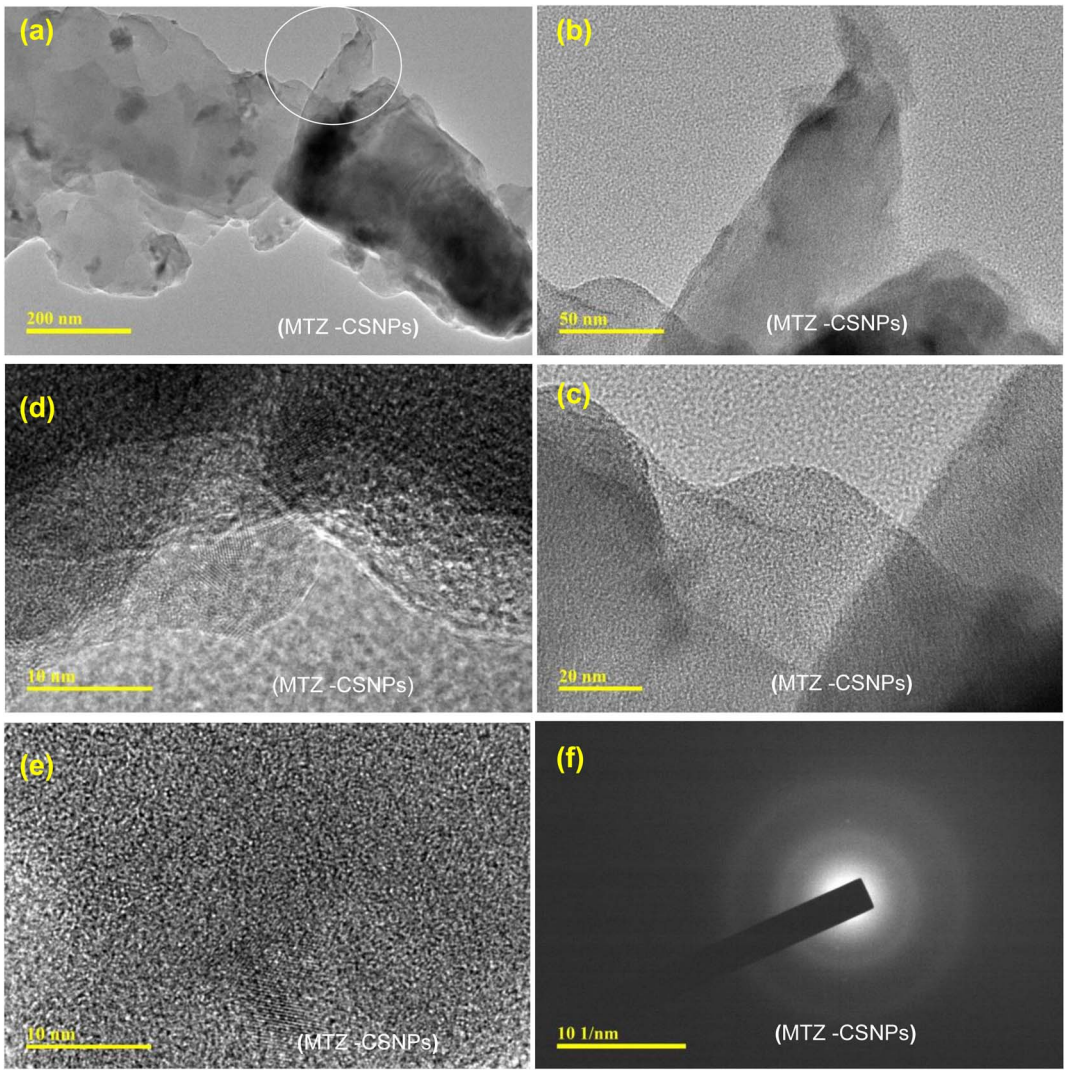

Fig. 4 TEM micrographs of metronidazole-loaded chitosan nanoparticles (MTZ-CSNPs): (a–e) MTZ-CSNPs at different magnifications, and (f) image showing the non-crystalline nature of the MTZ-CSNPs.

presented in Fig. 5. The TEM analysis at high magnification of the above three types of particles showed the increase in the particle size of the nanoparticles after loading CP and MTZ. Finally, on the basis of the SEM and TEM analyses, we could confirm that the drugs (CP and MTZ) were adsorbed on the surface of the chitosan nanoparticles as a drug carrier.

3.2.4. FTIR analysis. FTIR analysis was performed to confirm the interaction of the chitosan, TPP, and drugs. The FTIR spectra of CP, MTZ, CP-CSNPs, MTZ-CSNPs, and chitosan are presented in Fig. 6. Pure chitosan was confirmed by some characteristic peaks located at 3421, 1657, 1595, and 894 cm^{-1}. The band at 3421 cm^{-1} corresponded to the combined peaks of the NH_2 and OH groups' stretching vibrations in the chitosan, as shown in Fig. 6. The broadband between 1657 and 1595 cm^{-1} could be attributed to the C=O stretching vibration (amide I band) and the NH_2 group bending vibration.[35] The band at 894 cm^{-1} was related to the anhydro glucosidic ring. The bands at 2918 and 2878 cm^{-1} were related to C–H stretching, 2372 cm^{-1} was due to asymmetric C–N band stretching, 1379 cm^{-1} arose because of the asymmetric C–H bending of CH_2 group, and 1079 cm^{-1} was for the skeletal vibration involving C–O stretching. In the case of CP-CSNPs, the peak at 3421 cm^{-1} corresponding to the hydroxyl groups in pure chitosan was shifted to 3428 cm^{-1}, indicating that there could be some hydrogen bonding between the ciprofloxacin and chitosan nanoparticles. The bands at 1657 and 1595 cm^{-1} (amide I and amide II band), as clearly observed in pure chitosan, were decreased in the case of the CP-CSNPs, while two new absorption bands appeared at 1633 and 1536 cm^{-1} in the CP-CSNPs. This result indicated that the NH_3^+ groups of pure chitosan were crosslinked with the TPP groups of sodium polyphosphate, which helped to enhance both the inter- and intra-molecular interactions within the chitosan nanoparticles.[36] Besides, the bands at 2945 cm^{-1} (2918 cm^{-1} in chitosan) and 2878 cm^{-1} in CP-CSNPs were related to symmetric and asymmetric CH_3 stretching vibrations attributed to the pyranose ring of chitosan, while the band at 2358 cm^{-1} was due

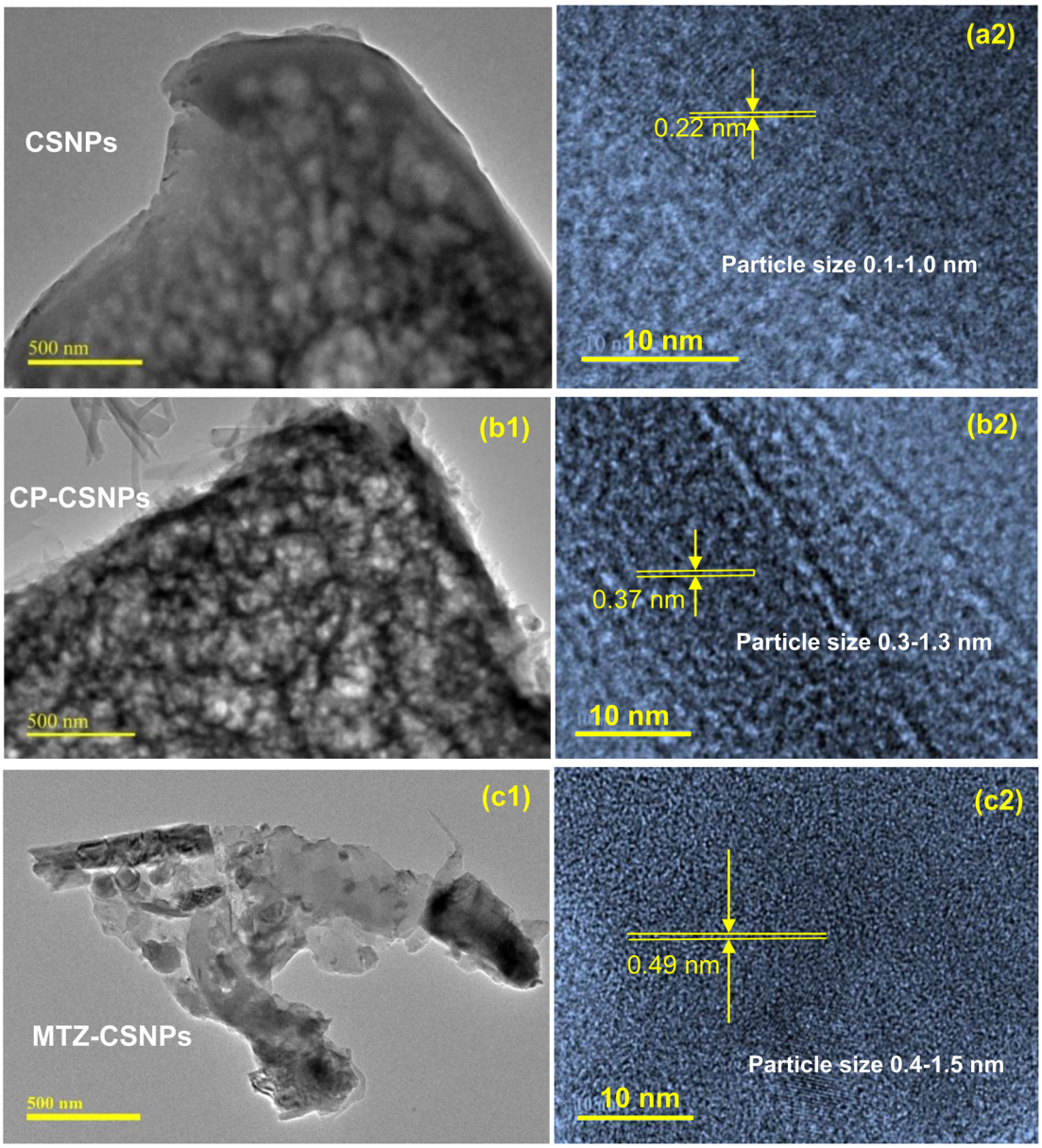

Fig. 5 Comparison of the particles size of the prepared (a1 and a2) CSNPs, (b1 and b2) CP-loaded CSNPs, and (c1 and c2) MTZ-loaded CSNPs at low and high magnifications, respectively.

to asymmetric stretching of the C–N band, which was found at 2372 cm^{-1} in pure chitosan, while the band at 1299–1155 cm^{-1} was related to the C–F band stretching of ciprofloxacin.

In the case of the metronidazole-loaded chitosan nanoparticles, the peak for –OH stretching was slightly shifted to 3434 from 3421 cm^{-1}, indicating the enhancement of hydrogen bonding in it. The peak for C=O stretching was found at 1642 cm^{-1} instead of 1657 cm^{-1}. The peak at around 1595 cm^{-1} was assigned to the NH bending vibration of amide II groups, which could be observed clearly in the pure chitosan but was decreased dramatically, and a new absorption band appeared at 1536 cm^{-1}, indicating the ammonium groups were crosslinked with tripolyphosphate molecules. The peak present at 1265 cm^{-1} corresponded to the N=O stretching of metronidazole in the nanoparticles.

Finally, the FTIR spectra of these two drug-loaded CSNPs showed that some peaks observed for pure chitosan were shifted, but the shifting was not very significant. So, it could be concluded that the drugs were loaded on to the chitosan nanoparticles without functional group interaction but there was electrostatic interaction between the drugs and chitosan nanoparticles.

3.2.5. XRD analysis. The XRD patterns of pure CP, MTZ, chitosan, CP-CSNPs, and MTZ-CSNPs were recorded between 5° and 70° 2θ diffraction angles and presented in Fig. 7. The XRD pattern of pure chitosan showed its semi crystalline properties with two peaks at $2\theta = 10.224°$ and 20.357° and a shoulder in 22.491°, in agreement with previous reports, and corresponding to the (020), (110), and (120) planes, respectively.[37,38]

In the case of CP-CSNPs, the decrease in % relative intensity of the (110) and (020) planes compared to the pure chitosan

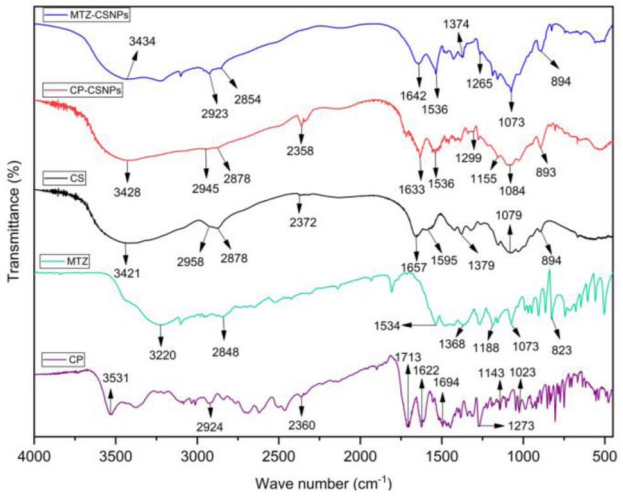

Fig. 6 FTIR spectra of chitosan, ciprofloxacin-loaded chitosan nanoparticles (CP-CSNPs), and metronidazole-loaded chitosan nanoparticles (MTZ-CSNPs).

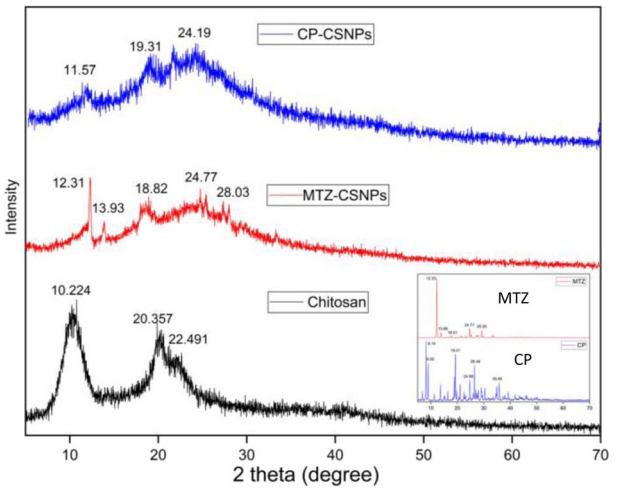

Fig. 7 XRD patterns of chitosan, MTZ-CSNPs, and CP-CSNPs. Inset shows the XRD patterns of pure CP and MTZ.

showed that the native chitosan had been successfully transformed into nanoparticles. Besides, these relatively broad and weaker peaks were found at $2\theta = 24.19$. In the case of MTZ-CSNPs these diffraction peaks were decreased after metronidazole loading, which indicates that the crystallinity was completely destroyed in the nanoparticles. At the same time, the metronidazole powder showed several sharp and intense peaks, which indicated the crystalline pattern of the drug. The XRD pattern of the metronidazole-loaded chitosan nanoparticles presented some small diffraction peaks for metronidazole at 2θ near 12°, 13°, 18°, 24°, and 28° when compared to free metronidazole (inset). However, these peaks were very broad and weaker and the other peaks had disappeared in the MTZ-CSNPs. This might be due to the loading of metronidazole on the nanoparticles, while the modification procedure destroyed the crystal structure of the metronidazole.

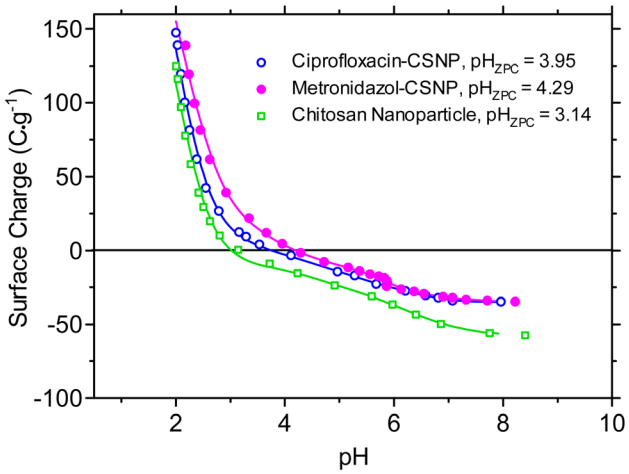

Fig. 8 Surface charges pH (pH_{ZPC}) or zeta potentials of chitosan, ciprofloxacin-loaded chitosan, and metronidazole-loaded chitosan nanoparticles.

3.3. Surface charge of the nanoparticles

The surface charge or zeta potential was determined from the measurement zero point of charge (ZPC or PZC), which is defined as the pH value where the surface positive and negative charges are equal.[31,32] The surface charges of the chitosan, ciprofloxacin-loaded chitosan, and metronidazole-loaded chitosan nanoparticles were determined from measurement of the pH as a function of acid–base titration.[31,32] Fig. 8 shows the variation of the surface charge density of chitosan, ciprofloxacin-loaded chitosan, and metronidazole-loaded chitosan nanoparticles as a function of pH in aqueous solution of 0.001 M $NaNO_3$. The point of zero charge (PZC) of chitosan, ciprofloxacin-loaded chitosan, and metronidazole-loaded chitosan nanoparticles was obtained from the intersection of σ_o *vs.* pH curves in Fig. 8. The values of pH_{PZC} for the chitosan, ciprofloxacin-loaded chitosan, and metronidazole-loaded chitosan nanoparticles were 3.15 ± 0.05, 3.95 ± 0.05, and 4.29 ± 0.05, respectively which indicate that at pH 3.15, 3.95, and 4.29, the surface charges of the chitosan, ciprofloxacin-loaded chitosan, and metronidazole-loaded chitosan nanoparticles, respectively, were zero (σ_o), and at pH values above or below the mentioned values, the above surfaces became negative or positive, respectively. The higher values of pH_{ZPC} for the ciprofloxacin-loaded chitosan and metronidazole-loaded chitosan nanoparticles than that for the chitosan nanoparticles suggested that the negative species of ciprofloxacin and metronidazole were electrostatically adsorbed on the chitosan nanoparticles.

3.4. *In vitro* drug release kinetic study

Fig. 9 presents the average cumulative percentage release of drugs (ciprofloxacin and metronidazole) from chitosan nanoparticles at various time intervals. In both cases, the *in vitro* release profile showed a biphasic pattern. These two phases in the release profile occurred due to "sudden release" and "sustained release". The sudden release or the initial rapid release

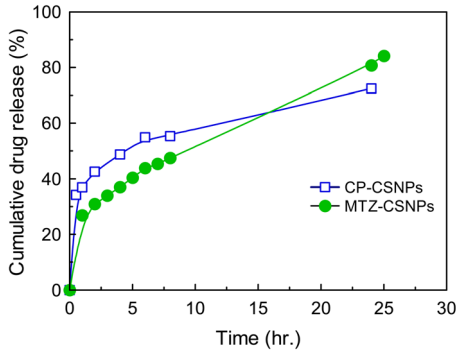

Fig. 9 Release profile of ciprofloxacin and metronidazole from CSNPs in PBS at pH = 7.4.

can be characterized as a "burst effect". From the release profile, it is very clear that the sudden release phase occurred in the first $\frac{1}{2}$ h for CP and 1 h for MTZ. As the rapid or burst release period ended, the rate of release of the drugs fell and the second phase then proceeded, which was the "sustained release" phase, which was slower than previous. These slower and sustained releases occurred throughout the incubation period.

Sustained drug release is the key strategy for reducing the systemic side effects of drugs in the human body associated with the frequency of drug administration and high drug concentrations. One of the most common methods used and studied to control drug release is encapsulation within a polymer matrix, which slows diffusion. However in the present study, the CSNPs were used for controlled release of the drug without encapsulation. Here, adsorption due to electrostatic interactions between the drugs and the CSNPs was the governing factor for drug release in this system.

To understand the release mechanism, we first examined the physical characteristics of this release system. The morphology and sizes of the nanoparticles were characterized by SEM and TEM analysis. The CP-CSNPs were spherical with diameters ranging from 0.3–1.3 nm, which were higher than the blank chitosan nanoparticles (0.1–1.0 nm). This was due to the adsorption of drugs on the surfaces of the nanoparticles according to the TEM analysis (Fig. 5). The size of the unmodified chitosan nanoparticles was too small to encapsulate the drug molecules into the nanoparticles matrix. However, our results showed very similar release profiles as for drugs encapsulated in nanoparticles, though they were was not encapsulated in the chitosan nanoparticles, indicating that another mechanism must be involved. To describe the release mechanism, we postulated that the sustained release that we observed was primarily caused by adsorption due to electrostatic interactions between the drugs and CSNPs.[39] We also postulated that initially the drugs are fully adsorbed on the nanoparticle surface. As the nanoparticle begins to degrade, the local pH of the system changes. At a certain threshold, the surface of the nanoparticles becomes neutral, weakening the electrostatic

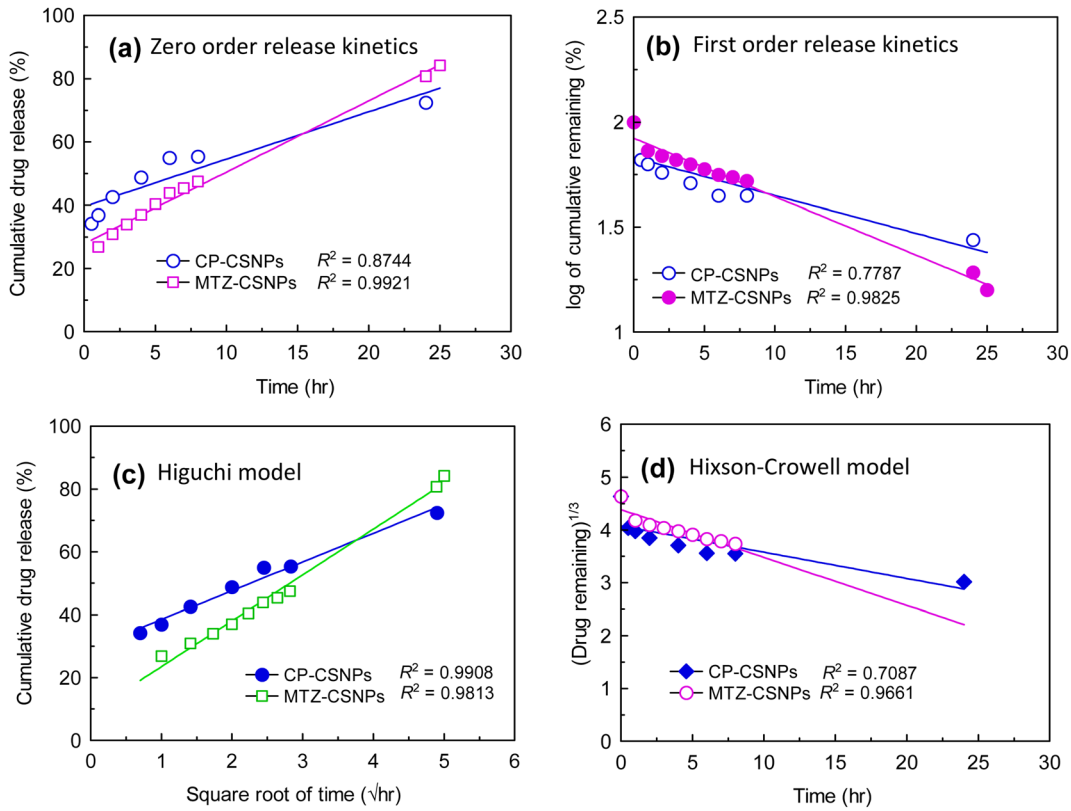

Fig. 10 Verification of drug release kinetics of drug-loaded CSNPs into PBS at pH = 7.4 using four different kinetic models: (a) zero-order release kinetics, (b) first-order release kinetics, (c) Higuchi square root model, and (d) Hixson-Crowell model.

Table 3 A comparison of the correlation of coefficients (R^2) for the fitness of different kinetic equation to the data of drug release from CSNPs in PBS of pH 7.0[a]

		R^2			
Samples	Saturation release (%)	Zero order	First order	Higuchi square root	Hixson-Crowell
CP-CSNPs	72 ± 3	0.874	0.779	0.991	0.709
MTZ-CSNPs	84 ± 3	0.992	0.983	0.981	0.966
Equation		$C_t = C_o + Kt$	$\log C = \log C_o - t/2.303$	$Q = K \times t^{1/2}$	$W_o^{1/3} - W_t^{1/3} = Kt$

[a] C_t is the amount of drug released at time t, C_o is the initial concentration of drug, C_t is the percentage of drug remaining at time t, Q is the cumulative amount of drug released in time t, W_o is the initial amount of drug in the pharmaceutical dosage form, W_t is the remaining amount of drug in the pharmaceutical dosage form at time t, and K is the rate constant of the individual release kinetics.

interactions and initiating release. Release can then be governed by nanoparticle degradation and drug diffusion or desorption, depending on the system. Finally, we can describe the mechanism of drug release from chitosan nanoparticles as usually involving polymer degradation, erosion, and diffusion of the drugs.[40] From the above results, it is clear that the chitosan nanoparticles had the effect of prolonging the release of these two drugs in the body.

The dissolution or release profile of drugs can be described by several mathematical models representing several release kinetics, as represented in Fig. 10. Data obtained from the *in vitro* release studies of the drug-loaded CSNPs were fitted to zero-order, first-order, Higuchi model, and Hixson-Crowell models. The optimum model was chosen on the basis of the highest correlation coefficient (R^2) value of these models.

Thus, the *in vitro* drug release profile applied in different mathematical models was evaluated by the correlation coefficient (R^2), as presented in Table 3. The highest degree of correlation coefficient determines the most suitable mathematical model that follows the drug release kinetics. From the above comparison, it was found that the Higuchi square root model showed a higher degree of correlation coefficient (R^2) than the other models.

So drug release was found to be best fitted by the Higuchi square root model ($R^2 = 0.991$ and 0.981 for ciprofloxacin and MTZ, respectively), which implies that the release of drug from matrix was a square root of the time dependent process and was diffusion controlled. Hence, the drug release profile of ciprofloxacin followed a diffusion mechanism.

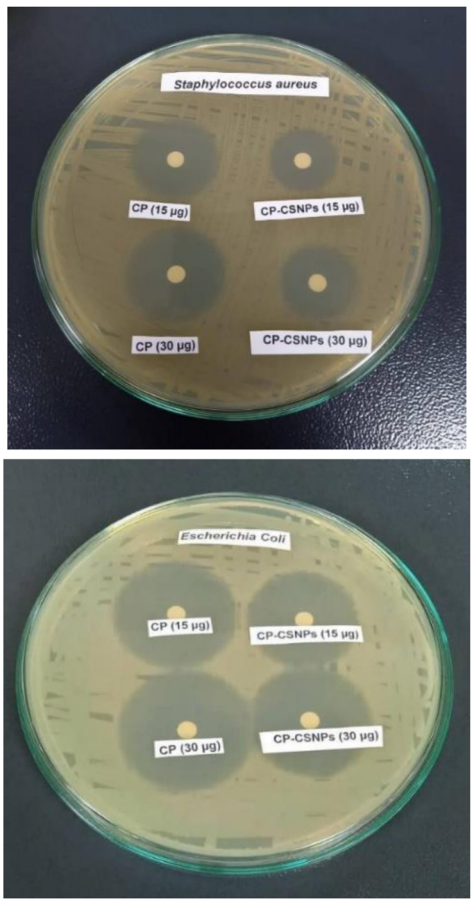

Fig. 11 Photographs of the zones of inhibition of free ciprofloxacin (CP) and ciprofloxacin-loaded nanoparticles (CP-CSNPs) against (a) *Staphylococcus aureus* and (b) *Escherichia coli*.

3.5. Antibacterial activity analysis

Microbiological studies were performed to observe the antibacterial activities of the ciprofloxacin-loaded chitosan nanoparticles (CP-CSNPs) against two types of bacteria, namely *Escherichia coli* (Gram negative) and *Staphylococcus aureus* (Gram positive).

3.5.1. Disk diffusion method. Results from the agar disk diffusion tests for assessing the antibacterial activities of CP-CSNPs and the free CP are illustrated in Fig. 11. The results showed that the CP-CSNPs inhibited the growth of both gram (+) and gram (−) bacterial strains. From Fig. 10(a and b), it could be seen that in terms of the surrounding clearing zone, both free CP and CP-CSNPs showed a very clear inhibitory effect against *E. coli* and *S. aureus*, indicating that the prepared CP-CSNPs were active against both types of bacteria. However under identical conditions, free ciprofloxacin showed a little higher zone of inhibition than CP-CSNPs against *S. aureus* and *E. coli*. This might be attributed to the slow diffusion of CP-CSNPs into the agar plate, as ciprofloxacin was associated with chitosan nanoparticles of higher molecular weight, and this result could be correlated to the extended release or slow

release of ciprofloxacin in a drug delivery system. In one study, CP-encapsulated PLGA nanoparticles showed lower antimicrobial activity than free CP in the *in vitro* analysis, which was because of the sustained release characteristics of the nanoparticles.[41] However, CP-encapsulated PLGA nanoparticles effectively inhibited the growth of bacteria due to the sustained release characteristics of nanoparticles than free CP in the case of the *in vivo* analysis. These suggest that CP-CSNPs may have superior effectiveness to inhibit the growth of bacteria *in vivo* due to its sustained release property.

3.5.2. MIC and MBC calculation by the macrodilution method. The antibacterial activity of CP-CSNPs was further analyzed by MIC and MBC determination using the macrodilution method. Both the MIC and MBC values of free CP and CP-CSNPs were the same against the Gram-negative bacteria *E. coli* and the values were <0.03 μg mL^{-1}. However, they showed an MIC value of 4 μg mL^{-1} and an MBC value of 64 μg mL^{-1} against the Gram-positive bacteria *S. aureus*.

The results imply that both free CP and CP-CSNPs showed similar effects in liquid media. Sobhani reported that CP-CSNPs showed better antibacterial activity than free CP,[42] whereas Jeong[41] suggested the opposite, whereby the *in vitro* antimicrobial activity of CP-encapsulated PLGA nanoparticles was relatively lower than that of free CP against *Escherichia coli*. However, our study showed no difference between the free antibiotic and antibiotic-loaded nanoparticles in liquid media. So, we can say that the loading of ciprofloxacin on chitosan nanoparticles did not show any negative effect on the antibacterial activity, rather it could be highly active for inhibiting bacterial growth *in vivo*.

4. Conclusion

In the current study, two different antibiotic drugs, namely ciprofloxacin and metronidazole, were successfully loaded on to chitosan nanoparticles prepared from the crosslinking of chitosan and TPP to investigate potential biomedical application. The drugs were loaded with high association efficiencies of 93 ± 3% and 90 ± 3% for ciprofloxacin and metronidazole, respectively. The CSNPs and CSNPs-loaded antibiotics were characterized by SEM, EDX, TEM, FTIR, and XRD. The morphology analysis of all the drug-loaded nanoparticles observed by SEM suggested that the particles were spherical in shape with homogeneous surfaces. The TEM analysis showed that the average diameters were increased in the drug-loaded nanoparticles compared to the blank one (0.1–1 nm), such as 0.3–1.3 nm and 0.4–1.5 nm for the CP-CSNPs and MTZ-CSNPs, respectively. These indicate the drugs adsorption on the surface of the nanoparticles rather than encapsulation. Comparison of the surface charges of the prepared nanoparticles and the small shifting of some characteristic peaks in the FTIR spectra of both the drug-loaded nanoparticles from pure chitosan indicated the existence of electrostatic interactions between the drugs and chitosan nanoparticles. The *in vitro* release profile study of CP-CSNPs and MTZ-CSNPs showed initial burst releases at $\frac{1}{2}$ h and 1 h followed by sustained release of 73 ± 3%, and 84 ± 3% of the drugs at 24 and 25 h, respectively, with the release profile governed by the Higuchi square root model for each case, which implies that the release of drugs was diffusion controlled. Due to the adsorption of drugs on the nanoparticles, the electrostatic interaction between the drugs and nanoparticles became the governing factor in sustaining the drug release effectively. Moreover, the antibacterial activity of CP-CSNPs observed by determination of the MIC and MBC showed similar results in the case of the loaded CP and free CP. This result implies that the loading of drugs on chitosan nanoparticles had no negative impact on the antibacterial activity. Furthermore, they may show better effectiveness to inhibit bacterial growth *in vivo* due to sustained release property according to several research studies. Finally, it can be concluded that the prepared nanoparticles have promising potential for use in drug delivery.

Data availability

The data used to support the findings of this study are included within the article.

Author contributions

Fatema Tuj Jahura: conceptualisation, methodology, investigation and writing. Farhana Khanam Ferdousi: formal analysis, resources and visualization. Abu Hena Mostofa Kamal: investigation of antibacterial activities and visualization. Anwar Ul-Hamid: TEM analysis and visualization. Md. Qamrul Ehsan: conceptualization, methodology, visualization and editing. Mohammad Abul Hossain: conceptualization, methodology, investigation, resources, writing, review editing, *etc.*

Conflicts of interest

There are no conflicts to declare.

Acknowledgements

The authors would like to acknowledge the Centennial Research Grant (CRG: 2020-2021) of Dhaka University. Fatema Tuj Jahura has given her thanks to the Bangabandhu Science and Technology Fellowship Trust, Bangladesh for the financial support.

References

1 M. P. Patel, R. R. Patel and J. K. Patel, *J. Pharm. Sci.*, 2010, **13**(4), 536–557.
2 D. Bhowmik, H. Gopinath, B. Kumar, S. Duraivel and K. Kumar, *Pharma Innov.*, 2012, **1**(10), 24–32.
3 T. Sagir, M. Huysal, M. Senel, S. Isık, N. Burgucu, O. Tabakoglu and M. Zaim, *J. Colloid Interface Sci.*, 2022, **625**, 711–721.
4 U. Garg, S. Chauhan, U. Nagaich and N. Jain, *Adv. Pharm. Bull.*, 2019, **9**(2), 195–204.
5 S. Laurent, D. Forge, M. Port, A. Roch, C. Robic, L. V. Elst and R. N. Muller, *Chem. Rev.*, 2008, **108**, 2064–2110.

6 A. Grenha, B. Seijo, C. Serra and C. R. Lopez, *Biomacromolecules*, 2007, **8**, 2072–2078.
7 *British Pharmacopia*, The stationary office, London, 2009, pp. 493–498.
8 D. Bhowmik, H. Gopinath, B. Kumar, S. Duraivel and K. Kumar, *Pharma Innov.*, 2012, **1**(10), 24–32.
9 E. Cevher, Z. Orhan, L. Mulazimoglu, D. Sensoy, M. Alper, A. Yildiz, *et al*, *Int. J. Pharm.*, 2006, **317**(2), 127–135.
10 M. Gomez-Burgaz, G. Torrado and S. Torrado, *Eur. J. Pharm. Biopharm.*, 2009, **73**(1), 130–139.
11 M. Kong, X. G. Chen, K. Xing and H. J. Park, *Int. J. Food Microbiol.*, 2010, **144**(1), 51–63.
12 K. S. V. K. Rao, P. R. Reddy, Y. I. Lee and C. Kim, *Carbohydr. Polym.*, 2012, **87**(1), 920–925.
13 L. H. Li, J. C. Deng, H. R. Deng, Z. L. Liu and X. L. Li, *Chem. Eng. J.*, 2010, **160**(1), 378–382.
14 A. I. Caco, F. Varanda, M. J. Pratas de Melo, A. M. A. Dias, R. Dohrn and I. M. Marrucho, *Ind. Eng. Chem. Res.*, 2008, **47**, 8083–8089.
15 F. Fawaz, F. Bonini, J. Maugein and A. M. Lagueny, *Int. J. Pharm.*, 1998, **168**, 255–259.
16 M.-E. Page-Clisson, H. Pinto-Alphandary, M. Ourevitch, A. Andremont and P. Couvreur, *J. Contr. Release*, 1998, **56**, 23–32.
17 K. Dillen, J. Vandervoort, G. Van den Mooter and A. Ludwig, *Int. J. Pharm.*, 2006, **314**, 72–82.
18 Y. C. Tseng, Y. Tabata, S. H. Hyon and Y. Ikada, *J. Biomed. Mater. Res.*, 1990, **24**, 1355–1367.
19 D. Jain and R. Banerjee, *J. Biomed. Mater. Res., Part B*, 2008, **86**(1), 105–112.
20 H. M. Ibrahim, M. K. El-Bisi, G. M. Taha and E. A. El-Alfy, *J. Appl. Pharmaceut. Sci.*, 2015, **5**(10), 85–90.
21 S. Latha, P. Selvamani, C. S. Kumar, P. Sharavanan, G. Suganya, V. S. Beniwal and P. R. Rao, *J. Magn. Magn Mater.*, 2009, **32**, 1580–1585.
22 G. Patel, R. B. Patel and H. R. Patel, *J. Sci. Technol.*, 2011, **6**(2), 33–45.
23 A. Allen, G. Flemstrom, A. Garner and E. Kivilaakso, *Physiol. Rev.*, 1993, **73**, 823–857.
24 M. George and T. E. Abraham, *J. Contr. Release*, 2006, **114**, 1–14.
25 J. D. Smart, I. W. Kellaway and H. E. Worthington, *J. Pharm. Pharmacol.*, 1998, **36**, 295–299.
26 V. Gonzalez, C. Guerrero and U. Ortiz, *J. Appl. Polym. Sci.*, 2000, **78**, 850–857.
27 M. R. Kasaai and M. Malaekeh, *Adv. Chitin Sci.*, 2003, **7**, 178–180.
28 A. A. Elzatahry and M. S. Mohy Eldin, *Polym. Adv. Technol.*, 2008, **19**(12), 1787–1791.
29 F. Tuj-Jahura, Department of Chemistry, PhD thesis, University of Dhaka, Bangladesh, 2022.
30 P. Calvo, J. L. Remunan-Lopez and A. M. J. Vila-Jato, *J. Appl. Polym. Sci.*, 1997, **63**(1), 125–132.
31 S. G. A. Parks and P. L. de Bruyn, *J. Phys. Chem.*, 1962, **66**, 967–973.
32 M. A. Hossain, PhD thesis, Kanazawa University, Japan, 2006.
33 I. Wiegand, K. Hilpert and R. E. W. Hancock, *Nat. Protoc.*, 2008, **3**(2), 163–170.
34 H. Ruchika, *Int. J. Sci. Res. Methodol.*, 2016, **4**(4), 1–17.
35 R. C. Nagarwal, P. N. Singh, S. Kant, P. Maiti and J. K. Pandit, *Chem. Pharm. Bull.*, 2011, **59**, 272–278.
36 L. Qi, Z. Xu, X. Jiang, C. Hu and X. Zou, *Carbohydr. Res.*, 2004, **339**(16), 2693–2700.
37 J. R. Anusha, A. T. Fleming, A. M. Valan, K. B. Chul, N. A. Al-Dhabi, K. H. Yu and R. C. Justin, *J. Adv. Res.*, 2016, **7**, 863–871.
38 E. M. A. Hejjaji, A. M. Smith and G. A. Morris, *Int. J. Biol. Macromol.*, 2017, **95**, 564–573.
39 H. F. G. Barbosa, D. S. Francisco, A. P. G. Ferreira and E. T. G. Cavalheiro, *Carbohydr. Polym.*, 2019, **225**, 115232.
40 M. M. Pakulska, I. E. Donaghue, J. M. Obermeyer, A. Tuladhar, C. K. McLaughlin, T. N. Shendruk and M. S. Shoichet, *Sci. Adv.*, 2016, **2**(5), e1600519.
41 Y. I. Jeong, H. S. Na, D. H. Seo, D. G. Kim, H. C. Lee and M. K. Jang, *Int. J. Pharm.*, 2008, **352**(1–2), 317–323.
42 Z. Sobhani, S. M. Samani, H. Montaseri and E. Khezri, *Adv. Pharm. Bull.*, 2017, **7**(3), 427–432.